Genetic and pharmacological reduction of CDK14 mitigates synucleinopathy

Authors: Jean-Louis A. Parmasad[1,2,†], Konrad M. Ricke[1,2,3†], Morgan G. Stykel[4], Brodie Buchner-Duby[4], Eric Lian[5,6], Benjamin Nguyen[1,2,3], Nathalie A. Lengacher[1,3,5], Haley M. Geertsma[1,2,3], Amanda Bruce[1,2], Steve M. Callaghan[1,2,3], Alvin Joselin[7], Julianna J. Tomlinson[1,3,5], Michael G. Schlossmacher[1,3,5], William L. Stanford[2,5,6], Patrik Brundin[8], Scott D. Ryan[4], and Maxime W.C. Rousseaux[1,2,3,6,*]

Affiliations:

[1] University of Ottawa Brain and Mind Research Institute, Ottawa, ON

[2] Department of Cellular and Molecular Medicine, University of Ottawa, Ottawa, ON

[3] Aligning Science Across Parkinson's (ASAP) Collaborative Research Network, Chevy Chase, MD

[4] Department of Molecular and Cellular Biology, University of Guelph, Guelph, ON

[5] Program in Neuroscience, Ottawa Hospital Research Institute, Ottawa, ON

[6] Ottawa Institute for Systems Biology, University of Ottawa, Ottawa, ON

[7] Hotchkiss Brain Institute, Department of Clinical Neurosciences, University of Calgary, Calgary, AB

[8] Parkinson's Disease Center, Department of Neurodegenerative Science, Van Andel Institute, Grand Rapids, MI

[†]Authors contributed equally

*Corresponding author. Email: max.rousseaux@uottawa.ca

One Sentence Summary:

Loss of CDK14 mitigates α-Synuclein pathology in Parkinson's disease (PD) mouse models and in human neurons, highlighting CDK14 as a druggable target for the treatment of PD.

Abstract:

Parkinson's disease (PD) is a debilitating neurodegenerative disease characterized by the loss of midbrain dopaminergic neurons (DaNs) and the abnormal accumulation of α-Synuclein (α-Syn) protein. Currently, no treatment can slow nor halt neurodegeneration. Multiplications and mutations of the α-Syn gene (*SNCA*) cause PD-associated syndromes and animal models that overexpress α-Syn replicate several features of PD. Decreasing total α-Syn levels, therefore, is an attractive approach to slow down neurodegeneration in patients with a 'synucleinopathy'. We previously performed a genetic screen for modifiers of α-Syn levels, and found CDK14, a kinase of largely unknown function as a regulator of α-Syn. To test the potential therapeutic effects of CDK14 reduction in PD, we decreased Cdk14 in two mouse models of synucleinopathy. We found that reduction of Cdk14 mitigated neuropathological and neurobehavioral sequelae associated with α-Syn overexpression. We further validated these findings in PD patient neurons. Finally, we leveraged the recent discovery of a covalent inhibitor of CDK14 to determine whether this target is pharmacologically tractable *ex vivo*. We found that in both mouse and human neurons, CDK14 inhibition decreases total and pathologically aggregated α-Syn. In summary, we suggest that CDK14 represents a novel therapeutic target for PD-associated synucleinopathy.

INTRODUCTION

Parkinson's disease (PD) is a neurodegenerative disease that affects over 10 million individuals worldwide (*1*,*2*). Individuals with PD present with motor symptoms such as bradykinesia, rigidity, shuffling gait, and resting tremor, as well as non-motor symptoms such as constipation, anosmia and sleep disturbances (*3*–*5*). Neuropathologically, typical PD is characterized by the loss of dopaminergic neurons (DaNs) in the substantia nigra pars compacta (SN) as well as the accumulation of α-synuclein (α-Syn) containing inclusions termed Lewy bodies and Lewy neurites (collectively: Lewy pathology) in surviving neurons (*6*–*8*). Current treatments address motor deficits, but are less effective on non-motor aspects of the disease and cannot slow down nor halt neurodegeneration in PD (*9*). Therefore, identifying new druggable targets for PD is clearly warranted. In addition to being abundantly present in Lewy pathology, point mutations and multiplications in the gene encoding α-Syn, *SNCA*, underlie monogenic variants of PD (*10*,*11*). Increased levels of *SNCA* mRNA are also observed in laser captured SN DaNs from PD patients (*12*), and animal models that overexpress α-Syn replicate several features of PD (*13*–*15*). Thus, there is a clear link between increased α-Syn dosage and PD pathogenesis, highlighting a crucial role of α-Syn in the manifestation of PD (*16*–*19*).

Since α-Syn dosage is linked to PD, decreasing total α-Syn levels may be a feasible approach to mitigate neurodegeneration in PD patients, regardless of whether oligomeric or fibrillar α-Syn is the toxic culprit. *Snca*-knockout (KO) mice are viable and fertile but display mild cognitive impairments, suggesting that a modest amount of cerebral α-Syn is required to accomplish its physiological role at the synapse (*20*,*21*). Titration of excessive α-Syn levels in a non-invasive manner would thus be beneficial in treating a chronic neurodegenerative disease like PD. Specifically, an orally available drug capable of mitigating α-Syn toxicity could offer a

minimally invasive approach, a feature particularly important in treating a chronic illness. A pooled RNAi screen investigating modifiers of α-Syn levels identified cyclin-dependent kinase 14 (CDK14, a.k.a. PFTK1) as a robust regulator of α-Syn in human neurons and *in vivo* (*22*). CDK14 is a brain expressed protein kinase with a largely unknown biological function (*23*). Its expression is upregulated in certain cancers, such as esophageal and colorectal cancer, for which it has generated attention as a therapeutic target (*24*,*25*). In fact, this has led to the recent development of FMF-04-159-2, a potent, covalent inhibitor of CDK14 (*26*).

Since reducing CDK14 leads to a mild reduction in endogenous α-Syn levels (*22*), we hypothesize that genetic and pharmacological inhibition of CDK14 reduces α-Syn pathology and PD-like phenotypes in mice and human cells. To test this hypothesis, we analyzed PD-like features in two PD mouse models (mice injected with preformed α-Syn fibrils, and α-Syn transgenic mice) with partial or full KO of *Cdk14*. Furthermore, using the recently developed specific CDK14 inhibitor, we tested if the pharmacological inhibition of CDK14 is sufficient to decrease α-Syn levels in rodent and human neurons. In summary, we show that decreasing CDK14 prevents α-Syn accumulation and ameliorates its downstream pathological consequences.

RESULTS

CDK14 ablation ameliorates motor impairment and α-Syn pathology in PFF-injected mice

Since PD is a chronic disease, inhibition of a candidate modifier would have to be safe, long term. We first tested the level of expression and consequence of depletion of Cdk14 in vivo. We found that Cdk14 was highly expressed in the brain (**fig. S1A**) and that Cdk14 nullizygous mice were viable, fertile, and exhibited normal brain morphology (*27*). We next asked whether silencing *Cdk14* is sufficient to mitigate behavioral and histological phenotypes observed in mice injected

with pathogenic α-Syn pre-formed fibrils (mouse PFFs; **Fig. 1A** and **B**; **fig. S1B** and **S2A**). Six months following intrastriatal injection of α-Syn PFFs, there is a stereotypic brain-wide accumulation of pS129 α-Syn – a marker of human synucleinopathies – in addition to SN DaNs loss and mild motor impairments (*28–30*). In our experimental paradigm, six months after PFF injection (at an age of 12 months), we found that PFF injected WT mice exhibited reduced forelimb force generation in the grip strength test when compared to their saline-treated counterparts ($P < 0.001$, Fig. 1B), similar to what has been previously reported (*29*,*30*). In contrast, the PFF-induced weakening of grip strength was not observed in *Cdk14*$^{+/-}$ or in *Cdk14*$^{-/-}$ mice. We did not observe PFF-mediated changes (in any genotype tested) in the other 8 behavioral tests conducted (including tests for cognitive and motor function). Furthermore, we noted that saline-injected *Cdk14*$^{+/-}$ and *Cdk14*$^{-/-}$ mice consistently performed like their WT counterparts in each test, suggesting that chronic Cdk14 reduction is not deleterious to the brain (**fig. S2A**).

Cdk14 loss lowers signal of cerebral pS129 α-Syn reactivity after intrastriatal PFF injection

We next turned to histology to determine the relative pathological burden of accumulated α-Syn throughout the brain of mice injected with PFFs. We stained for synucleinopathy-linked pS129 α-Syn in the brain of WT mice and found high amounts of pS129 α-Syn-positive cells in the PFF-injected hemisphere (ipsilateral to the injection, IL), which were absent in saline-injected controls ($P < 0.01$, data not shown). We then mapped the distribution of α-Syn pathology at three different rostrocaudal levels near the injection site (relative to bregma: +0.98 mm, +0.26 mm and -1.34 mm) and found an overall blunting of pS129 α-Syn-positive pathology in the PFF-injected *Cdk14*$^{+/-}$ and *Cdk14*$^{-/-}$ mice when compared to their WT littermates (**Fig. 1C**). This was particularly evident IL at the level of the somatomotor cortex (bregma +0.26 mm) and in other areas of the cortex (**Fig.**

1C). Previous reports have shown that α-Syn PFFs can induce nigrostriatal degeneration over time (*28–30*). We stained for tyrosine hydroxylase (TH) at the injection site in the striatum but did not observe a decrease of TH+ dopamine fibers in mice injected with PFFs (**fig. S2B**).

Loss of Cdk14 mitigates PD-associated phenotypes in mice overexpressing human α-Syn

We next asked whether partial loss of Cdk14 is sufficient to reduce α-Syn-induced phenotypes in a more aggressive model of synucleinopathy. To do so, we crossed *Cdk14* heterozygous mice (*Cdk14*$^{+/-}$) to wildtype (WT) or to α-Syn-overexpressing transgenic (*mThy1-SNCA*, a.k.a. "*α-Syn TG*") mice (**Fig. 2A**) (*31*,*32*). These mice exhibit a 3-5-fold overexpression of human α-Syn and exhibit a host of behavioral and neuropathological features reminiscent of PD within a few months of age (*32*). We only examined male mice as the *α-Syn TG* transgene is located on the X chromosome leading to X-inactivation and mosaic phenotypes in female mice. We tested whether reduction of Cdk14 affects PD-like behavioral symptoms in 3-month-old *α-Syn TG* mice (**Fig. 2**). We found that, in every test assayed, *α-Syn TG* mice exhibited strong motor deficits when compared to their WT littermates (**Fig. 2B, C** and **D**). In the pole test, which is routinely used to measure PD-like motor impairment in mice (*33*,*34*), we observed that mice harboring both the *α-Syn TG* allele and a loss of function *Cdk14* allele (*α-Syn TG; Cdk14*$^{+/-}$) did not display any motor dysfunction (**Fig. 2B**). This finding is particularly interesting given the high degree of α-Syn overexpression compared to the modest reduction (50%) of Cdk14. In the beam break and nesting tests *α-Syn TG; Cdk14*$^{+/-}$ mice displayed similar phenotype manifestations as their *α-Syn TG* littermates (**Fig. 2C** and **D**).

We then measured the levels of α-Syn and phosphorylated α-Syn (pS129) isolated from hemibrains of 5-month-old mice (**Fig. 2E**). The reduction of Cdk14 induced a surprising increase

in pS129 α-Syn levels in the soluble fraction of *α-Syn TG mice*, without affecting total α-Syn dosage. However, in the insoluble protein fraction of this PD mouse line, Cdk14 loss did not alter pS129 α-Syn levels. Instead Cdk14 loss led to a mild, yet significant reduction of total α-Syn. These data suggest that reducing Cdk14 alters α-Syn metabolism, resulting in a net decrease of aggregated α-Syn protein levels in the diseased mouse brain.

Decreasing Cdk14 mitigates neurodegeneration in mice overexpressing human α-Syn

α-Syn TG mice develop cortical and hippocampal cell loss as well as corresponding astrogliosis and pS129 α-Syn accumulation (*31*,*35–37*) . We asked whether a 50% reduction of Cdk14 would be sufficient to alter brain pathologies in 5-month-old *α-Syn TG* mice. We found that α-Syn overexpression induced robust neuronal loss in the hippocampus (CA3 region) and cortex (Layer V). In contrast, double mutant (*α-Syn TG; Cdk14*$^{+/-}$) littermates did not develop this level of neurodegeneration in these brain regions (**Fig. 3A** and **B**). We measured the presence of aggregate-associated α-Syn species via pS129 α-Syn staining and the degree of astrogliosis via GFAP staining. We found that *α-Syn TG* mice developed pS129-positive α-Syn pathology and astrogliosis, regardless of the *Cdk14* genotype (**fig. S3A** and **B**).

Knockdown of CDK14 decreases α-Syn and pS129 α-Syn levels in human neurons

Having observed the benefits of Cdk14 depletion in two mouse models of PD with different degrees of α-Syn pathology, we next tested whether this benefit translates to human neurons. We infected DaNs derived from a PD patient carrying an A53T mutation in α-Syn (*38*) as well as its isogenic control with lentiviruses carrying Cas9/sgRNAs against *CDK14*. Neurons infected with sgRNAs targeting either exon 3 (E3) or exon 8 (E8) of *CDK14*, exhibited approximately 50% of

the CDK14 levels of the control cultures (**Fig. 3C**). We found that A53T mutant cells showed a marked increase of pS129 α-Syn compared to isogenic controls and, in parallel, PD neurons with silenced *CDK14* exhibited significantly lower pS129 levels (**Fig. 3C**).

Pharmacological targeting of CDK14 decreases α-Syn levels and mitigates its pathogenic accumulation

As kinases are typically druggable targets which can be inhibited in non-invasive ways (*39*), we next asked whether CDK14 pharmacological inhibition would be a tractable route for decreasing α-Syn levels. We used a recently developed CDK14 covalent inhibitor (FMF-04-159-2) (*26*) to test whether acute depletion of CDK14 decreased α-Syn levels. We found that in HEK293T cells, CDK14 inhibition induced a strong reduction in endogenous α-Syn protein levels (**Fig 4A**). We asked whether CDK14 inhibition-induced α-Syn clearance was mediated by the ubiquitin proteasome system (UPS) or autophagy. We found that blocking the UPS or autophagy did not affect the reduction of α-Syn dosage, induced by CDK14 inhibition (**fig. S3C**). Rather, blocking CDK14 resulted in decreased *SNCA* transcript levels. Moreover, we observed that CDK14 itself was being cleared via the UPS. We next asked if CDK14 inhibition decreases α-Syn levels in hESC-derived cortical neurons. CDK14 inhibition caused a dose-dependent reduction in total α-Syn concentration by ELISA (**Fig. 4B)**. Lastly, we tested whether application of this inhibitor was sufficient to block α-Syn pathology in rat primary neuronal cultures treated with α-Syn PFFs. We found that Cdk14 inhibition markedly reduced the PFF-induced elevation of high molecular weight α-Syn species over a five-day period (**Fig. 4C**). Thus, pharmacological treatment of isolated human neurons or PFF-challenged rat neurons with a CDK14 inhibitor showed consistent reduction in α-Syn protein.

DISCUSSION

α-Syn is increasingly considered a valid experimental therapeutic target for PD, based on clinical genetic and neuropathological evidence, as well as animal and cell culture studies. *SNCA* gene mutations or amplifications resulting in α-Syn pathology are tightly linked to PD pathogenesis. Moreover, α-Syn is a major constituent of Lewy-like structures, the pathological hallmark of PD and related synucleinopathies. Thus, targeting α-Syn has been a major thrust in the pharmaceutical realm. One aspect of α-Syn pathology that has been difficult to overcome is the notion that different states of its post-translational modification or aggregation differentially affect disease pathogenesis: a clear image has yet to emerge as to the real culprit of α-Syn toxicity. Although novel strategies such as anti-sense oligonucleotides, immunotherapy and small molecule inhibitors of α-Syn aggregation are being explored (*40*), finding a target that can be pharmacologically inhibited still holds potential as a minimally invasive and simple strategy to lower α-Syn levels – especially when such treatment course would be made over several decades. Indeed, a growing body of evidence suggests that α-Syn may play a role not only at the presynaptic space, but also in the immune system (*41–43*). Therefore, careful titration of its levels may be more clinically pertinent. As a result, we asked whether candidates that are more amenable to traditional pharmacology (e.g. kinases) could regulate α-Syn dosage, irrespective of its aggregation status. Our previous studies identified a handful of these modifiers including TRIM28 and DCLK1 (*8*,*22*,*36*,*44*). Here, we study a heretofore unexplored target for disease modification in pre-clinical models of PD: CDK14.

Building on our initial identification of CDK14 as a potential regulator of α-Syn levels (*22*), we show that reduction of CDK14 is well tolerated and causes a reduction in pathogenic α-Syn accumulation in murine and human models of synucleinopathy. Genetic suppression of *Cdk14* ameliorates the accumulation of pathologically linked pS129 α-Syn in the cortex of PFF-injected

mice and halts the development of PD-related motor defects. Moreover, we show that halving Cdk14 in the brains of α-Syn overexpressing mice is sufficient to blunt the development of PD-associated neurodegenerative phenotypes. Importantly, the genetic reduction of CDK14 in DaNs derived from an individual with synucleinopathy shows equal promise in preventing phenotypic development. Lastly, we show that a newly developed CDK14 inhibitor, FMF-04-159-2, effectively inhibits CDK14, decreases α-Syn levels in hESC-derived human neurons, and mitigates PFF-induced α-Syn pathology in rat cortical neurons. Collectively, these results show that CDK14 is a pharmacologically tractable target for synucleinopathy.

We found that while the net effect of decreasing CDK14 on reducing α-Syn levels and its associated phenotypes were consistent, its effect on α-Syn phosphorylation was context-dependent. For instance, genetic reduction of CDK14 resulted in decreased pS129 α-Syn in both the PFF model as well as the human DaNs derived from the *SNCA-A53T* carrier. In contrast, partial reduction of Cdk14 resulted in an increase in soluble pS129 α-Syn in the *α-Syn TG* line, despite decreasing total aggregated α-Syn and blunting neurodegenerative phenotypes. We surmise that Cdk14 mediates its effect toward α-Syn not directly via its phosphorylation. Indeed, we could not detect any kinase activity of recombinant CDK14 toward wild-type α-Syn *in vitro* (data not shown). Thus, we hypothesize that loss or inhibition of CDK14 causes a decrease in α-Syn through an unknown mediator, affecting maintenance of *SNCA* transcript and α-Syn protein levels. Future studies will help refine the mechanism whereby CDK14 regulates α-Syn.

Our results examining the genetic and pharmacological reduction of CDK14 in PD models pioneer future pre-clinical studies. In all behavioral experiments conducted, $Cdk14^{-/-}$ mice were indistinguishable from WT mice (**Fig 1B** and **fig S1**), implying that *Cdk14* loss is not deleterious *in vivo*. This is supported by human genetics where loss of *CDK14* appears to be well tolerated

(probability of loss of function intolerance [pLI] = 0; gnomAD database, CDK14 | gnomAD v2.1.1), (*45*)). Moreover, the activity of the CDK14 inhibitor in human neurons appears to be high, affecting CDK14 (and thus α-Syn metabolism) in the nanomolar range. While FMF-04-159-2 has yet to be tested in animal models, our cell culture experiments provide proof-of-principle for its potential role in the reduction of α-Syn pathology. Further preclinical experiments will address the safety of FMF-04-159-2 in animals and test whether the drug rescues PD-like models of synucleinopathies; potentially paving the way for its application in human subjects.

In sum, we show that CDK14 inhibition causes a decrease total α-Syn concentrations under both *ex vivo* and *in vivo* conditions and consequently ameliorates α-Syn-driven phenotypes in mouse and human PD models. Given the strong evidence linking α-Syn levels to PD pathogenesis, we conclude that targeting CDK14 function holds promise as a potentially disease-modifying approach to treat PD.

MATERIALS AND METHODS

Study design

The objective of this study was to analyze whether reduction of CDK14 decreases α-Syn pathology *in vitro* and *in vivo*. To test if Cdk14 reduction mitigates α-Syn-induced toxicity in PD mouse models, we injected preformed mouse α-Syn fibrils (PFFs) in the brains of *Cdk14*$^{+/-}$, *Cdk14*$^{-/-}$ and WT littermate mice. In addition, we combined mice with genetic reduction of *Cdk14* with mice overexpressing full-length human α-Syn to test whether genetic reduction of *Cdk14* ameliorates PD-like characteristics. Dosage of α-Syn protein was analyzed in human neurons from *SNCA A53T* carriers with reduced CDK14 levels. Furthermore, we asked if pharmacological inhibition of CDK14 affects α-Syn levels in rodent and human cells and applied the CDK14 inhibitor FMF-04-

159-2 to cultured rat and hESC-derived human cortical neurons. Sample size was established prior to study onset and were generally picked based on previous data from the literature using these models. All procedures with mice were performed in accordance with the guidelines of the Canadian Council on Animal Care and stipulations of the Ethics Board and the Animal Care Committee at the University of Ottawa.

Mouse strains

Cdk14$^{+/-}$ mice were generated by the Gene Targeting and Transgenic Facility of Texas A&M Institute for Genomic Medicine (TIGM), on a mixed (129/SvEvBrd x C57BL/6) background (as described previously (*27*). *Cdk14*$^{+/-}$ mice were backcrossed 14 times to the C57Bl/6NCrl background prior to experimentation (PFF or genetic interaction). *Cdk14*$^{+/-}$ mice were paired to generate *Cdk14*$^{-/-}$ mice. Since the *α-Syn TG* transgene is located on the X chromosome (*32*), *α-Syn TG; Cdk14*$^{+/-}$ X chromosomal females were paired with *Cdk14*$^{+/-}$ males. Resulting WT, *α-Syn TG*, *Cdk14*$^{+/-}$ and *α-Syn TG; Cdk14*$^{+/-}$ males were used for experimental procedures. Only males were used for experiments as female mice undergo X chromosome inactivation, resulting in variable phenotypes. Behavioral experiments were performed on 3-month-old mice.

Stereotactic PFF injections

Endotoxin-free recombinant mouse α-Syn fibril preparations were stored at -80ºC before usage (*46*,*47*). On the day of the stereotactic injections, fibrils were thawed and sonicated in a sonicator water bath to generate PFFs (Covaris S220, 18 W peak incident power, 20% duty factor, 50 cycles per burst, 150 seconds). For transmission electron microscopy (TEM) analysis (Transmission Electron Microscopy Core Facility, University of Ottawa) 0.2 mg/mL PFF samples were stained

with Uranyl Acetate and imaged on a FEI Tecnai G2 Spirit Twin TEM. 6-month-old mice were deeply anesthetized with isoflurane, and 1 µL PFFs (5 mg/mL) or sterile saline (0.9% NaCl) was unilaterally delivered into the dorsal striatum of the right hemisphere at these coordinates relative to bregma: -2 mm medial-lateral; +0.2 mm antero-posterior and -2.6 mm dorso-ventral. Injections were performed using a 2 µL syringe (Hamilton, Reno, NV, USA) at a rate of 0.1 µL/min with the needle left in place for at least 3 minutes before its slow withdrawal. After surgery, animals were monitored, and post-surgical care was provided. Behavioral experiments were performed 6 months post injection, followed by the collection of the brains at 7 months post injection.

Behavioral experiments

Grip strength tests were performed by holding the mice at an automatic grip strength meter (Chatillon DFE II, Columbus Instruments) allowing them to grip the grid of the device with their fore- and hindlimbs. Then, mice were gently pulled back by their tail until they released the grip. Force exerted by the mouse during its removal from the grid, as measured by gram force (g), was evaluated 5 times per mouse. For nesting behavior tests, mice were singly caged overnight (16 hours) with a 5x5cm cotton nestlet in a clean cage. Produced nests were scored on a scale from 1-5 as previously described (*48*). For beam break tests single mice were placed in the testing apparatus (Omnitech Electronics) for 24 hours with standard rodent chow and water *ad libitum*. Locomotion is presented as distance travelled. Pole tests were performed by placing the mice on the top of a vertical pole (8 mm diameter and 55 cm height) with a rough surface. Mice were placed with their head facing the room ceiling and the time required for turning was recorded. The mean time to turn was calculated from 5 consecutive trials for each mouse.

304 **Tissue harvesting and processing**

305 For biochemical approaches with hemibrains from 5-month-old *α-Syn TG Cdk14*$^{+/-}$ *mice and their*
306 *littermates*, mice were anesthetized with isoflurane (Fresenius Kabi, CP0406V2), and decapitated.
307 Brains were isolated and hemibrains were lysed 1:4 (w/v) in NETN buffer (250 mM NaCl, 5 mM
308 EDTA pH 8, 0.5% NP-40, 50 mM Tris-HCL, pH 8 in ddH_2O) with protease (GenDEPOT, P3100)
309 and phosphatase inhibitors (GenDEPOT, P3200) using Dounce homogenizers. Lysates were
310 cleared by centrifugation at 18,000 x *g* for 20 minutes at 4°C. Cleared lysates were transferred to
311 a new, low protein binding tube, and the pellets were frozen at -80°C for subsequent analysis. To
312 isolate insoluble proteins, pellets were thawed and resuspended in 88% formic acid 1:1 (w/v).
313 Samples were left to incubate for 1 hr at room temperature, then diluted to 22 % formic acid content
314 with PBS. Samples were dried overnight at 60 °C in an Eppendorf Vacufuge concentrator. Dried
315 protein was resuspended in phosphate-buffered saline (PBS) with protease and phosphatase
316 inhibitors at 1:4 (w/v) based on the initial hemibrain weight. Samples were sonicated at 20 % 10
317 sec ON, 10 sec OFF for 4 minutes total time, using an FB120 sonicator (Fisher Scientific) with Cl-
318 18 probe (Qsonica), while kept on ice.
319 For immunohistology with paraffin sections, mice were anesthetized with 120 mg/kg Euthanyl
320 (DIN00141704) and intracardially perfused with 10 mL of PBS, followed by 20 mL of 10 %
321 Buffered Formalin Phosphate (Fisher Scientific, SF100-4). Brains were isolated and fixed in 10 %
322 Buffered Formalin Phosphate at 4°C for at least 24 hours. After dehydration by 70 %, 80 %, 90 %
323 and 100 % ethanol and clearing by Xylenes, brains were infiltrated and embedded in paraffin
324 (Louise Pelletier Histology Core Facility, University of Ottawa). Brains were sectioned at 5 µm.
325

326 **SDS-PAGE and mouse protein immunoblots**

4X Laemmli buffer (Bio-Rad, 1610747) with 20 % 2-mercaptoethanol (Bio-Rad, 1610710) was added to cleared protein and boiled at 95 °C for 5 minutes. Protein samples were loaded on a 12 % SDS-PAGE gel in the Mini-PROTEAN Tetra Cell (Bio-Rad, 165-8000). Protein was then transferred to a 0.2 µm nitrocellulose membrane (Bio-Rad, 1620112) using the Mini Trans-Blot Electrophoretic Transfer Cell (Bio-Rad, 1703930) in Tris-Glycine buffer with 10 % methanol (Fisher Scientific, A412P) at 340mA for 90 minutes at 4 °C. Membranes were then blocked in 5 % milk in 1X TBS-T for 1hr at room temperature followed by overnight incubation in primary antibody against pSer129 α-Syn (1:2,000, Abcam, 51253), α-Syn (1:2,000, BD Biosciences, 610787), CDK14 (1:500, Santa Cruz, sc50475) and GAPDH (1:40,000, Proteintech, 60004-1-Ig) diluted in 2% BSA, 0.02% NaN_3 in 1X TBS-T. Next, membranes were washed in TBS-T, followed by incubation in secondary antibody (peroxidase-conjugated donkey anti-rabbit IgG, Cedarlane, 711-035-152 or donkey anti-mouse IgG, Cedarlane, 715-035-150, both at 1:10,000 diluted in 5% milk in TBS-T) for 1 hour at room temperature. Membranes were washed again in TBS-T, bathed in enhanced chemiluminescent reagent (Bio-Rad, 1705061), imaged using the ImageQuant LAS 4100 Imaging system (GE) and quantified using Image Lab 6.1 software (Bio-Rad Laboratories).

Immunohistology

For Diaminobenzidine (DAB) antibody staining, paraffin sections were deparaffinized in xylenes and rehydrated in a series of decreasing ethanol (100 %, 90 %, 70 %, 50 %) followed by antigen retrieval in sodium citrate buffer (2.94 g sodium citrate, 0.5 mL Tween-20 in 1 L PBS, pH6) at 95°C for 20 min and quenching of endogenous peroxidase with 0.9 % H_2O_2 in PBS for 10 min. Sections were blocked in blocking buffer (0.1 % Triton X-100, 10 % normal horse serum in PBS) and incubated in primary antibody (pSer129 α-Syn, 1:500, Abcam, 51253 or tyrosine hydroxylase,

1:1,000, Sigma-Aldrich, AB152) overnight at 4 ºC. Then, sections were incubated in secondary antibody (donkey anti-rabbit biotin-conjugated, Jackson ImmunoResearch, 711-065-152, 1:250 in blocking buffer) for 2 hours and tertiary antibody solution (streptavidin-horseradish peroxidase conjugated, 1:500 in blocking buffer, Sigma-Aldrich, RPN1231V) for 2 h before being exposed to DAB (Vector, SK-4100) for 10 minutes. Hematoxylin counterstaining was conducted using the H&E Staining Kit (Abcam, ab245880) as per manufacturer's instructions. Stained sections were dehydrated in a series of ethanol and xylenes solutions, followed by mounting sections with Permount (Fisher Scientific, SP15-100).

For immunofluorescence antibody staining, after the deparaffinization/dehydration, antigen retrieval and blocking, sections were incubated in primary antibody (NeuN, 1:500, EMD Millipore, MAB377 or GFAP, 1:1,000, Synaptic Systems, 173 004) in blocking buffer overnight at 4ºC. Next, sections were incubated in secondary antibody (donkey anti-mouse IgG (H+L) Alexa Fluor™ 568, Thermo Fisher Scientific, A10037, for NeuN and goat anti-guinea pig IgG (H+L) Alexa Fluor™ 488, for GFAP) together with DAPI (Sigma-Aldrich, D9542) for 1 hour at RT, followed by mounting sections with fluorescence mounting medium (Agilent, S302380-2). Brightfield and epifluorescence micrographs were acquired using an Axio Scan Z1 Slide Scanner (20x objective, Louise Pelletier Histology Core Facility) and a Zeiss AxioImager M2 (10x objective, Cell Biology and Image Acquisition Core Facility, University of Ottawa) and analyzed using ImageJ (National Institute of Health, 1.52p) with 2-3 sections per mouse by a blinded investigator. Heatmaps were generated by counting pS129 α-Syn positive cells in defined regions of the brain (http://atlas.brain-map.org), normalized to the area occupied by the region and resulting cell densities were expressed as hues of red.

373 **Cell culture**

374 Cells were kept at 37 °C, 5 % O_2, 10 % CO_2. HEK293T cells (ATCC, CRL-3216) were cultured
375 in Dulbecco's modified Eagle's medium (DMEM, Wisent Bioproducts, 319-015-CL),
376 supplemented with 10% FBS (Sigma-Aldrich, F1051) and antibiotic/antimitotic (Thermo
377 Scientific, 15240062).

378

379 **hiPSC culture, neuronal differentiation, and Cas9-mediated gene editing**

380 hiPSC isogenic lines (Female) and hESC isogenic lines (Male) were generated as described by
381 (*38*). Genotypes of hESC-derived WT, A53T, and E46K as well as hiPSC-derived Corrected and
382 A53T cell lines were confirmed by restriction digest of genomic DNA (*38*). hiPSCs were cultured
383 as previously described (*49*) with slight modifications. Briefly, pluripotent cells were plated in
384 mTeSR (Stem Cell Technologies) and media was changed daily. The colonies were manually
385 passaged weekly. Differentiation of hPSCs into A9-type DaNs was performed by following a floor
386 plate differentiation paradigm (*49*,*50*). Immediately preceding differentiation, the colonies were
387 dissociated into a single cell suspension using HyQTase. hPSCs were collected and re-plated at
388 $4x10^4$ cells/cm^2 on Matrigel (BD)-coated tissue culture dishes for differentiation. Floor-plate
389 induction was carried out using hESC-medium containing knockout serum replacement (KSR),
390 LDN193189 (100 nM), SB431542 (10 µM), Sonic Hedgehog (SHH) C25II (100 ng/mL,
391 Purmorphamine (2 µM), Fibroblast growth factor 8 (FGF8; 100 ng/mL), and CHIR99021 (3 µM).
392 On day 5 of differentiation, KSR medium was incrementally shifted to N2 medium (25%, 50%,
393 75%) every 2 days. On day 11, the medium was changed to Neurobasal/B27/Glutamax
394 supplemented with CHIR. On day 13, CHIR was replaced with Brain Derived Neurotrophic Factor
395 (BDNF; 20 ng/mL), ascorbic acid (0.2 mM), Glial Derived Neurotrophic Factor (GDNF; 20

ng/mL), transforming growth factor beta 3 (TGFβ3; 1 ng/mL), dibutyryl cAMP (dbcAMP; 0.5 mM), and DAPT (10 μM) for 9 days. On day 20, cells were dissociated using HyQTase and re-plated under high cell density $4x10^5$ cells/cm^2 in terminal differentiation medium (NB/B27 + BDNF, ascorbic acid, GDNF, dbcAMP, TGFβ3 and DAPT) also referred to as DA Neuron (DAN)-Medium, on dishes pre-coated with poly-ornithine (15 μg/mL)/laminin (1 μg/mL)/fibronectin (2 μg/mL). Cells were differentiated for up to 60 DIV, with analysis being performed at DIV14, DIV 45 and/or DIV 60. At D10D and D14D or differentiation, hPSC cultures were transduced with lentivirus containing Cas9 (lentiCRISPR v2, addgene, plasmid #52961) with the following gRNAs: non-targeting (5'-CGCTTCCGCGGCCCGTTCAA-3'), CDK14 exon 3 (5'-GCAAAGAGTCACCTAAAGTT-3') and exon 8 (5'-TGTGCAAAATATAACGCTGG-3'). From D10D-D14D media was supplemented with 0.1 μM compound E (AlfaAesar, J65131). At D18D, cells were replated onto poly-ornithine (15 μg/mL)/laminin (1 μg/mL)/fibronectin (2 μg/mL) coated plates. Cells were maintained in DAN-medium (DMEM/F12, 200uM Ascorbic Acid, 0.5 mM dbcAMP, 20 ng/mL BDNF, 20 ng/mL GDNF, 1 ng/mL TGFb3, and 1 % Anti-Anti) for 6-7 weeks where lysates were then collected for protein analysis.

hESC culture, neuronal differentiation and *in vitro* CDK14 inhibitor treatment

Dishes for hESC cultures were coated with 0.15 mg/mL growth factor reduced Matrigel (Corning, 354230) in DMEM/F-12 (Thermo Fisher Scientific, 11320033) for 1 hour at room temperature prior to cell seeding. H9 hESCs (WiCell, WA09) were seeded as colonies and maintained in mTeSR Plus (StemCell Technologies, 05825). Neural progenitor cell (NPC) differentiation was initiated when the hESC cultures reached 90% confluence, by replacing growth medium with Knockout Serum Replacement (KSR) medium (414 mL Knockout-DMEM (Thermo Fisher

Scientific, 10829018), 75 mL Knockout-serum replacement (Thermo Fisher Scientific, 10828028), 5 mL Glutamax (Thermo Fisher Scientific, 35050061), 5 mL MEM-NEAA (Thermo Fisher Scientific, 11140050), 500 µL 2-mercaptoethanol (Thermo Fisher Scientific, 21985023), 500 µL Gentamicin (Wisent Bioproducts 450-135), 10 µM SB431542 (Tocris, 1614) and 500 nM LDN-193189 (Stemgent, 04-0074). Differentiation medium was replaced daily on days 4 and 5 by 75:25 KSR:N2 medium (486.5 mL DMEM/F-12 (Thermo Fisher Scientific, 11320033), 5 mL 15% glucose, 5 mL N2 supplement (Thermo Fisher Scientific, 17502048), 500 µL 20 mg/mL human insulin (Wisent Bioproducts, 511-016-CM), 2.5 mL 1M HEPES (Thermo Fisher Scientific, 15630080), 500 µL Gentamicin), on days 6 and 7 by 50:50 KSR:N2, on days 8 and 9 by 25:75 KSR:N2 and on days 10 and 11 by N2 medium containing 500 nM LDN-193189. On day 12, differentiated NPCs were treated with Y-27632 (Tocris, 1254) for 4 hours, dissociated with Accutase (Stemcell Technologies, 07922) and seeded into Matrigel coated dishes containing Neural Induction Medium (NIM, 244 mL DMEM/F12, 244 mL Neurobasal medium (Thermo Fisher Scientific, 21103049), 2.5 mL N2 Supplement, 5 mL B-27 Supplement (Thermo Fisher Scientific, 17504044), 2.5 mL GlutaMAX™ (Thermo Fisher Scientific, 35050061), 125 µL 20 mg/mL human insulin, 500 µL 20 µg/mL FGF2 (StemBeads, SB500), 10 µL 1 mg/mL hEGF (Millipore Sigma E9644) and 500 µL Gentamicin) for expansion. NPCs were passaged at full confluence a minimum of one time before neuronal differentiation.

For NPC-neuronal differentiation culture dishes were coated with 0.001 % Poly-L-ornithine (Millipore Sigma, P4957) at 4 °C overnight, followed by 25 µg/mL laminin (Millipore Sigma, L2020) for 2 h at room temperature. NPCs were treated with Y-27632 for 4 hours, dissociated with Accutase and seeded at a density of 20,000 cells/cm^2 in NIM. Neuronal differentiation was initiated when NPCs reached 70% confluence by replacing growth medium

with neuronal differentiation medium (244 mL DMEM/F-12 medium, 244 mL Neurobasal medium, 2.5 mL N2 supplement, 5 mL B27 supplement, 200 µL 50 µg/ml BDNF (Peprotech, 450-02), 200 µL 50 µg/ml GDNF (Peprotech, 450-10), 250 mg dibutyryl cyclic-AMP (Millipore Sigma, D0627), 500 µL 100 M L-ascorbic acid (FujiFim Wako Chemicals, 323-44822), and 500 µL Gentamicin). Cells were fed every 3 days for 18 days to obtain immature neuronal networks. FMF-04-159-2 (R&D Systems, 7158) was dissolved in DMSO (Fisher Scientific, BP231) and applied in cell culture medium to hESC-derived neurons for 72 hours and to HEK293T cells for 18 hours. HEK293T cells were treated with 500 nM of FMF-04-159-2 together with 200 nM of Bafilomycin A1 (in DMSO, NEB, 54645S) or 1 µM of MG-132 (in DMSO, EMD Millipore, 474790) for 18 hours to inhibit autophagy or the UPS, respectively. For protein analysis cells were washed with cold PBS, scraped, and collected in low protein binding microcentrifuge tubes (Thermo Scientific, 90410). Cells were pelleted by centrifugation at 1,000 x g for 5 minutes at 4°C. The supernatant was aspirated, and the cells were lysed in cold RIPA buffer (50 mM Tris, pH 7.5, 150 mM NaCl, 0.1% SDS, 0.5% sodium deoxycholate; 1% NP-40, 5 mM EDTA, pH 8.0) with protease and phosphatase inhibitors. Cell lysates were incubated on ice for 20 minutes, with vortexing every 5 minutes. Lysates were centrifuged at 18,000 x *g* for 20 minutes at 4 °C to pellet cell debris. Autophagic activity was monitored by immunoblots for LC3B (Novus Biologicals, NB100-2220). Proteasome activity was monitored by immunoblots for poly-ubiquitinated proteins (anti-ubiquitin P4D1, Cell Signaling Technology, 3136).

RNA extraction and Reverse Transcription Quantitative PCR (RTqPCR)

RNA from HEK293T cells was extracted using the RNeasy Mini Kit (Qiagen, 74106) following the manufacturer's guidelines. cDNA was synthesized using the 5X All-in-One RT Master Mix

Kit (BioBasic, HRT025-10). RTqPCR was conducted using the Green-2-Go qPCR Master Mix (BioBasic, QPCR004-S) with 25 ng DNA per reaction and primers targeting *GAPDH* (Forward: 5'-CGACCACTTTGTCAAGCTCA-3', Reverse: 5'-TTACTCCTTGGAGGCCATGT-3'), *HPRT1* (Forward: 5'-GACCAGTCAACAGGGGACAT-3', Reverse: 5'-GTGTCAATTATATCTTCCACAATCAAG-3') and *SNCA* (Forward: 5'-ACCAAACAGGGTGTGGCAGAAG-3', Reverse: 5'- CTTGCTCTTTGGTCTTCTCAGCC-3'). Reactions were performed in a BioRad CFX96 thermocycler (protocol: 95 ºC for 5 minutes, 40 cycles of 95 ºC for 15 seconds and 60 ºC for 60 seconds, followed by melting curve). *SNCA* Ct values were standardized to the average of *GAPDH* and *HPRT1* Ct values and *SNCA* expression was displayed as fold change of the DMSO control.

ELISA

ELISA α-Syn protein quantification was performed as previously described (*41*,*51*). 384-well MaxiSorp plates (Nunc, Inc) were coated with capturing antibody (α-Syn, BD Biosciences, 610787) diluted 1:500 in coating buffer ($NaHCO_3$ with 0.2 % NaN3, pH 9.6) overnight at 4 °C. Following 3 washes with PBS/0.05 % Tween-20 (PBST), plates were blocked for 1 hour at 37 °C in blocking buffer (1.125 % fish skin gelatin; PBS-T). After 3 washes, samples were loaded in duplicates and incubated at RT for 2 hours. Biotinylated hSA4 antibody (in-house antibody) was generated using 200 µg Sulfo-NHS-LC Biotin (Pierce), diluted 1:200 in blocking buffer and added to the plate for 1 hour at 37 °C. Following 5 washes, ExtrAvidin phosphatase (Sigma E2636) diluted in blocking buffer was applied for 30 min at 37 °C. Color development was carried out by using fast-p-nitrophenyl phosphate (Sigma, N1891) and monitored at 405 nm every 2.5 min for up

to 60 min. Saturation kinetics were examined for identification of time point(s) where standards and sample dilutions were in the log phase.

Primary rat neurons, human α-Syn PFFs and protein analysis

Cortical neurons were harvested from the E18 Sprague Dawley rat embryos (Charles River). The harvested cortical tissue was digested using 17 U/mg Papain followed by mechanical dissociated by gentle trituration through a glass flamed Pasteur pipet. The cells were seeded into plates coated 24 hours prior to dissection with Poly-D-Lysine (0.15 mg/mL). The cells were incubated at 37 °C, 7.5 % CO_2 until collection. Every 3 to 4 days, a 50% media change was performed (2 % B27 supplement, 1 % antibiotic/antimycotic, 0.7 % BSA Fraction V, 0.1 % β-mercaptoethanol in HEPES-buffered DMEM/F12). Where required, cells were exposed to 100 nM FMF-04-159-2 (Bio-Techne, 7158/10) dissolved in DMSO, at 14 DIV, and again at the subsequent feed (18 DIV). At 14 DIV, cells were exposed to either 1 µg/mL human α-Syn PFFs, or 1 µg/mL monomeric α-Syn. Cell lysates were collected at D0 (no exposure), D1, D3, and D5 post PFF or monomeric exposure. Human α-Syn protein was isolated from BL21-CodonPlus (DE3)-RIPL competent cells transformed with pET21a-alpha-synuclein and purified by Reversed-phase HPLC. PFFs were then generated as previously described (*52*). Purified α-Syn (5 µg/mL in PBS) was incubated at 37°C with constant shaking for 7 days, then aliquot and stored at -80 °C. Prior to use, PFFs were thawed and diluted in PBS, then subjected to sonication (20 % amplitude, 30 seconds; 1 second on, 1 second off) and added to neuronal media for exposure to neurons at a concentration of 1 µg/mL for 24 hours. Following the incubation, cell lysates were collected in 150 µL ice-cold RIPA buffer containing phosphatase and protease inhibitors (1 mM aprotinin, 1 mM sodium orthovanadate, 1 nM sodium fluoride, and 10 mM phenylmethylsulfonyl fluoride). Samples were homogenized

using a 18G needle, left on ice to rest for 15 minutes, and then centrifuged at 14,000 *g* to remove any cellular debris. Using the BioRad DC Protein Assay kit, the protein concentration of each sample was quantified following the manufacturers guidelines. SDS-PAGE was performed using a 12.5 % resolving gels and a 4 % stacking gels, and gels were run for 15 minutes at 80 V followed by approximately 1.5 hours at 110 V. The gels were transferred onto 0.2 μM nitrocellulose membranes at 35 V and 4°C overnight. Following the transfer, the membranes were blocked for 1 hour at room temperature using blocking buffer (5 % non-fat dry milk in 1X PBS) with constant agitation. Primary antibodies were prepared in blocking buffer containing 0.1 % Tween20 and were probed overnight at 4 °C under constant agitation (CDK14, 1:1,000, Santa Cruz, sc50475, TH, 1:1,000, Pel Freeze, P40101, a-Syn, 1:1,000, BD, BD 610787, pS129 a-Syn, 1:500, abcam, ab51253, β-Actin, 1:1,000, rabbit, Biolegend, 622101 or mouse, Sigma, A5411, βIII-Tubulin, 1:5,000, rabbit, Biolegend, 802001). Following primary antibody incubation, membranes were rinsed using 1XPBS containing 0.1 % Tween20 and subsequently re-blocked using the blocking buffer. The membranes were then probed with secondary antibody for 1 hour at RT in blocking buffer containing 0.1 % Tween20 (Goat anti-Mouse IgG (H+L) Secondary Antibody, HRP (Thermo Fisher Scientific, 31430); Goat anti-Rabbit IgG (H+L) Secondary Antibody, HRP (Thermo Fisher Scientific, 31460); Li-Cor infrared conjugated secondary/ IRDye 800RD Donkey anti-Rabbit IgG antibody (LI-COR Biosciences, 926-32211) at dilutions of 1:2,000). The membranes were rinsed to remove any residual blocking buffer using 1X PBS containing 0.1 % Tween20. If HRP-conjugated secondary antibodies were used, membranes were probed for 5 minutes with clarity Western enhanced chemiluminescence blotting substrate (Bio-Rad) and visualized with photosensitive film. For LiCOR-secondary antibodies, membranes were visualized with a LiCOR Odyssey Fc.

Statistics

Statistical analysis was performed using GraphPad Prism version 9.2.0. Quantified data are visualized as mean + standard error of the mean. Unpaired student's *t* tests were used for two-group comparisons. Data affected by one or two factors were analyzed by one-way or two-way analysis of variance (ANOVA), respectively, followed by Bonferroni *post hoc* comparisons (unless otherwise stated in the figure legend) when at least one of the main factors or the interaction was significant. A significance level of 0.05 was accepted for all tests. Asterisks mark *P* values ≤ 0.05 (*), ≤ 0.01 (**), ≤ 0.001 (***), or ≤ 0.001 (****).

References and Notes

1. Selvaraj S, Piramanayagam S. Impact of gene mutation in the development of Parkinson's disease. Genes Dis. 2019;6(2):120–8.
2. Mhyre TR, Boyd JT, Hamill RW, Maguire-Zeiss KA. Parkinson's disease. Subcell Biochem. 2012;65:389–455.
3. Sveinbjornsdottir S. The clinical symptoms of Parkinson's disease. J Neurochem. 2016;139:318–24.
4. Mazzoni P, Shabbott B, Cortés JC. Motor control abnormalities in Parkinson's disease. Cold Spring Harb Perspect Med. 2012;2(6):1–17.
5. Berardelli A, Rothwell JC, Thompson PD, Hallett M. Pathophysiology of bradykinesia in Parkinson's disease. Brain. 2001 Nov;124(11):2131–46.
6. Mor DE, Ischiropoulos H. The Convergence of Dopamine and α-Synuclein: Implications for Parkinson's Disease. J Exp Neurosci. 2018 Mar;12:1179069518761360–1179069518761360.
7. Fujiwara H, Hasegawa M, Dohmae N, Kawashima A, Masliah E, Goldberg MS, et al. α-Synuclein is phosphorylated in synucleinopathy lesions. Nat Cell Biol [Internet]. 2002;4(2):160–4. Available from: https://doi.org/10.1038/ncb748
8. Vázquez-Vélez GE, Gonzales KA, Revelli J-P, Adamski CJ, Alavi Naini F, Bajić A, et al. Doublecortin-like Kinase 1 Regulates α-Synuclein Levels and Toxicity. J Neurosci [Internet]. 2020;40(2):459. Available from: http://www.jneurosci.org/content/40/2/459.abstract
9. Rousseaux MWC, Shulman JM, Jankovic J. Progress toward an integrated understanding of Parkinson's disease [version 1; peer review: 2 approved]. F1000Research [Internet]. 2017;6(1121). Available from: http://openr.es/9uu
10. Campêlo CL das C, Silva RH. Genetic Variants in SNCA and the Risk of Sporadic

Parkinson's Disease and Clinical Outcomes: A Review. Parkinsons Dis [Internet]. 2017/07/11. 2017;2017:4318416. Available from: https://pubmed.ncbi.nlm.nih.gov/28781905

11. Singleton AB, Farrer M, Johnson J, Singleton A, Hague S, Kachergus J, et al. α-Synuclein Locus Triplication Causes Parkinson's Disease. Science (80-) [Internet]. 2003;302(5646):841. Available from: http://science.sciencemag.org/content/302/5646/841.abstract
12. Gründemann J, Schlaudraff F, Haeckel O, Liss B. Elevated α-synuclein mRNA levels in individual UV-laser-microdissected dopaminergic substantia nigra neurons in idiopathic Parkinson's disease . Nucleic Acids Res [Internet]. 2008 Mar 10;36(7):e38–e38. Available from: https://doi.org/10.1093/nar/gkn084
13. Feany MB, Bender WW. A Drosophila model of Parkinson's disease. Nature [Internet]. 2000;404(6776):394–8. Available from: https://doi.org/10.1038/35006074
14. Masliah E, Rockenstein E, Veinbergs I, Mallory M, Hashimoto M, Takeda A, et al. Dopaminergic Loss and Inclusion Body Formation in α-Synuclein Mice: Implications for Neurodegenerative Disorders. Science (80-) [Internet]. 2000;287(5456):1265. Available from: http://science.sciencemag.org/content/287/5456/1265.abstract
15. Lakso M, Vartiainen S, Moilanen A-M, Sirviö J, Thomas JH, Nass R, et al. Dopaminergic neuronal loss and motor deficits in Caenorhabditis elegans overexpressing human α-synuclein. J Neurochem [Internet]. 2003 Jul 1;86(1):165–72. Available from: https://doi.org/10.1046/j.1471-4159.2003.01809.x
16. Chu Y, Kordower JH. Age-associated increases of α-synuclein in monkeys and humans are associated with nigrostriatal dopamine depletion: Is this the target for Parkinson's disease? Neurobiol Dis [Internet]. 2007;25(1):134–49. Available from: http://www.sciencedirect.com/science/article/pii/S0969996106002191
17. Polymeropoulos MH, Lavedan C, Leroy E, Ide SE, Dehejia A, Dutra A, et al. Mutation in the alpha-synuclein gene identified in families with Parkinson's disease. Science. 1997 Jun;276(5321):2045–7.
18. Stefanis L. α-Synuclein in Parkinson's Disease. Cold Spring Harb Perspect Med [Internet]. 2012 Feb 1;2(2). Available from: http://perspectivesinmedicine.cshlp.org/content/2/2/a009399.abstract
19. Sulzer D, Edwards RH. The physiological role of α-synuclein and its relationship to Parkinson's Disease. J Neurochem [Internet]. 2019 Sep 1;150(5):475–86. Available from: https://doi.org/10.1111/jnc.14810
20. Becket G-H, Manuela P, Megumi M-T, Ling D, M. WA, H. NE, et al. αβγ-Synuclein triple knockout mice reveal age-dependent neuronal dysfunction. Proc Natl Acad Sci [Internet]. 2010 Nov 9;107(45):19573–8. Available from: https://doi.org/10.1073/pnas.1005005107
21. Kokhan VS, Afanasyeva MA, Van'kin GI. α-Synuclein knockout mice have cognitive impairments. Behav Brain Res. 2012;231(1):226–30.
22. Rousseaux MWC, Vázquez-Vélez GE, Al-Ramahi I, Jeong H-H, Bajić A, Revelli J-P, et al. A Druggable Genome Screen Identifies Modifiers of α-Synuclein Levels via a Tiered Cross-Species Validation Approach. J Neurosci [Internet]. 2018;38(43):9286. Available from: http://www.jneurosci.org/content/38/43/9286.abstract
23. Shu F, Lv S, Qin Y, Ma X, Wang X, Peng X, et al. Functional characterization of human PFTK1 as a cyclin-dependent kinase. Proc Natl Acad Sci U S A [Internet]. 2007/05/21.

2007 May 29;104(22):9248–53. Available from: https://pubmed.ncbi.nlm.nih.gov/17517622

24. Chen L, Wang Y, Jiang W, Ni R, Wang Y, Ni S. CDK14 involvement in proliferation migration and invasion of esophageal cancer. Ann Transl Med [Internet]. 2019 Nov;7(22):681. Available from: https://pubmed.ncbi.nlm.nih.gov/31930082
25. Zhou Y, Rideout WM, Bressel A, Yalavarthi S, Zi T, Potz D, et al. Spontaneous genomic alterations in a chimeric model of colorectal cancer enable metastasis and guide effective combinatorial therapy. PLoS One. 2014;9(8):1–13.
26. Ferguson FM, Doctor ZM, Ficarro SB, Browne CM, Marto JA, Johnson JL, et al. Discovery of Covalent CDK14 Inhibitors with Pan-TAIRE Family Specificity. Cell Chem Biol [Internet]. 2019;26(6):804-817.e12. Available from: http://www.sciencedirect.com/science/article/pii/S2451945619300704
27. Rodríguez González Y, Kamkar F, Jafar-nejad P, Wang S, Qu D, Sanchez Alvarez L, et al. PFTK1 kinase regulates axogenesis during development via RhoA activation. bioRxiv [Internet]. 2022 Jan 1;2022.01.11.475789. Available from: http://biorxiv.org/content/early/2022/03/10/2022.01.11.475789.abstract
28. Luk KC, Kehm V, Carroll J, Zhang B, O'Brien P, Trojanowski JQ, et al. Pathological α-Synuclein Transmission Initiates Parkinson-like Neurodegeneration in Nontransgenic Mice. Science (80-) [Internet]. 2012;338(6109):949. Available from: http://science.sciencemag.org/content/338/6109/949.abstract
29. Mao X, Ou MT, Karuppagounder SS, Kam T-I, Yin X, Xiong Y, et al. Pathological α-synuclein transmission initiated by binding lymphocyte-activation gene 3. Science [Internet]. 2016 Sep 30;353(6307):aah3374. Available from: https://pubmed.ncbi.nlm.nih.gov/27708076
30. Kam T-I, Mao X, Park H, Chou S-C, Karuppagounder SS, Umanah GE, et al. Poly(ADP-ribose) drives pathologic α-synuclein neurodegeneration in Parkinson's disease. Science [Internet]. 2018 Nov 2;362(6414):eaat8407. Available from: https://pubmed.ncbi.nlm.nih.gov/30385548
31. Rockenstein E, Mallory M, Hashimoto M, Song D, Shults CW, Lang I, et al. Differential neuropathological alterations in transgenic mice expressing α-synuclein from the platelet-derived growth factor and Thy-1 promoters. J Neurosci Res. 2002 Jun;68(5):568–78.
32. Chesselet M-F, Richter F, Zhu C, Magen I, Watson MB, Subramaniam SR. A progressive mouse model of Parkinson's disease: the Thy1-aSyn ("Line 61") mice. Neurotherapeutics [Internet]. 2012;9(2):297–314. Available from: https://pubmed.ncbi.nlm.nih.gov/22350713
33. Matsuura K, Kabuto H, Makino H, Ogawa N. Pole test is a useful method for evaluating the mouse movement disorder caused by striatal dopamine depletion. J Neurosci Methods [Internet]. 1997;73(1):45–8. Available from: https://www.sciencedirect.com/science/article/pii/S016502709602211X
34. Sedelis M, Schwarting RKW, Huston JP. Behavioral phenotyping of the MPTP mouse model of Parkinson's disease. Behav Brain Res [Internet]. 2001;125(1):109–25. Available from: https://www.sciencedirect.com/science/article/pii/S0166432801003096
35. Dhungel N, Eleuteri S, Li L, Kramer NJ, Chartron JW, Spencer B, et al. Parkinson's Disease Genes VPS35 and EIF4G1 Interact Genetically and Converge on α-Synuclein. Neuron [Internet]. 2015;85(1):76–87. Available from: https://www.sciencedirect.com/science/article/pii/S0896627314010812

36. Rousseaux MWC, de Haro M, Lasagna-Reeves CA, De Maio A, Park J, Jafar-Nejad P, et al. TRIM28 regulates the nuclear accumulation and toxicity of both alpha-synuclein and tau. Ackerman SL, editor. Elife [Internet]. 2016;5:e19809. Available from: https://doi.org/10.7554/eLife.19809
37. Rockenstein E, Clarke J, Viel C, Panarello N, Treleaven CM, Kim C, et al. Glucocerebrosidase modulates cognitive and motor activities in murine models of Parkinson's disease. Hum Mol Genet [Internet]. 2016 Jul 1;25(13):2645–60. Available from: https://doi.org/10.1093/hmg/ddw124
38. Soldner F, Laganière J, Cheng AW, Hockemeyer D, Gao Q, Alagappan R, et al. Generation of Isogenic Pluripotent Stem Cells Differing Exclusively at Two Early Onset Parkinson Point Mutations. Cell [Internet]. 2011;146(2):318–31. Available from: https://www.sciencedirect.com/science/article/pii/S0092867411006611
39. Bhullar KS, Lagarón NO, McGowan EM, Parmar I, Jha A, Hubbard BP, et al. Kinase-targeted cancer therapies: progress, challenges and future directions. Mol Cancer [Internet]. 2018 Feb 19;17(1):48. Available from: https://pubmed.ncbi.nlm.nih.gov/29455673
40. Gouda NA, Elkamhawy A, Cho J. Emerging Therapeutic Strategies for Parkinson’s Disease and Future Prospects: A 2021 Update. Vol. 10, Biomedicines . 2022.
41. Tomlinson JJ, Shutinoski B, Dong L, Meng F, Elleithy D, Lengacher NA, et al. Holocranohistochemistry enables the visualization of α-synuclein expression in the murine olfactory system and discovery of its systemic anti-microbial effects. J Neural Transm [Internet]. 2017;124(6):721–38. Available from: https://doi.org/10.1007/s00702-017-1726-7
42. L. BE, Aaron M, D. SK, S. BK, Mastooreh C, E. MT, et al. Alpha-Synuclein Expression Restricts RNA Viral Infections in the Brain. J Virol [Internet]. 2022 May 2;90(6):2767–82. Available from: https://doi.org/10.1128/JVI.02949-15
43. Allen Reish HE, Standaert DG. Role of α-synuclein in inducing innate and adaptive immunity in Parkinson disease. J Parkinsons Dis [Internet]. 2015;5(1):1–19. Available from: https://pubmed.ncbi.nlm.nih.gov/25588354
44. Rousseaux MWC, Revelli J-P, Vázquez-Vélez GE, Kim J-Y, Craigen E, Gonzales K, et al. Depleting Trim28 in adult mice is well tolerated and reduces levels of α-synuclein and tau. Ackerman SL, editor. Elife [Internet]. 2018;7:e36768. Available from: https://doi.org/10.7554/eLife.36768
45. Karczewski KJ, Francioli LC, Tiao G, Cummings BB, Alföldi J, Wang Q, et al. The mutational constraint spectrum quantified from variation in 141,456 humans. Nature [Internet]. 2020;581(7809):434–43. Available from: https://doi.org/10.1038/s41586-020-2308-7
46. Volpicelli-Daley LA, Luk KC, Patel TP, Tanik SA, Riddle DM, Stieber A, et al. Exogenous α-synuclein fibrils induce Lewy body pathology leading to synaptic dysfunction and neuron death. Neuron [Internet]. 2011 Oct 6;72(1):57–71. Available from: https://pubmed.ncbi.nlm.nih.gov/21982369
47. Polinski NK, Volpicelli-Daley LA, Sortwell CE, Luk KC, Cremades N, Gottler LM, et al. Best Practices for Generating and Using Alpha-Synuclein Pre-Formed Fibrils to Model Parkinson's Disease in Rodents. J Parkinsons Dis [Internet]. 2018;8(2):303–22. Available from: https://pubmed.ncbi.nlm.nih.gov/29400668

48. Deacon R. Assessing burrowing, nest construction, and hoarding in mice. J Vis Exp [Internet]. 2012 Jan 5;(59):e2607–e2607. Available from: https://pubmed.ncbi.nlm.nih.gov/22258546
49. Ryan SD, Dolatabadi N, Chan SF, Zhang X, Akhtar MW, Parker J, et al. Isogenic Human iPSC Parkinson's Model Shows Nitrosative Stress-Induced Dysfunction in MEF2-PGC1α Transcription. Cell [Internet]. 2013;155(6):1351–64. Available from: http://www.sciencedirect.com/science/article/pii/S0092867413014220
50. Kriks S, Shim J-W, Piao J, Ganat YM, Wakeman DR, Xie Z, et al. Dopamine neurons derived from human ES cells efficiently engraft in animal models of Parkinson's disease. Nature [Internet]. 2011;480(7378):547–51. Available from: https://doi.org/10.1038/nature10648
51. Bojan S, Mansoureh H, E. HI, Michaela L, Juliana R, Nathalie L, et al. Lrrk2 alleles modulate inflammation during microbial infection of mice in a sex-dependent manner. Sci Transl Med [Internet]. 2019 Sep 25;11(511):eaas9292. Available from: https://doi.org/10.1126/scitranslmed.aas9292
52. Volpicelli-Daley LA, Luk KC, Lee VM-Y. Addition of exogenous α-synuclein preformed fibrils to primary neuronal cultures to seed recruitment of endogenous α-synuclein to Lewy body and Lewy neurite–like aggregates. Nat Protoc [Internet]. 2014;9(9):2135–46. Available from: https://doi.org/10.1038/nprot.2014.143

Acknowledgments:

The authors thank Drs. Robert Rissman (UCSD), Eliezer Masliah (UCSD/NIA) and David Park (University of Calgary) for sharing the mutant mice used in this study. We thank Dr. G. Vázquez-Vélez (Washington University) for his critical appraisal of the manuscript. The authors also thank the following Core facilities from the University of Ottawa and the Ottawa Hospital Research Institute for use of their facility, equipment, and expertise: Animal Behaviour and Physiology Core, Cell Biology and Imaging Acquisition Core, StemCore Laboratories and Louise Pelletier Histology Core. Schemes were generated using biorender (https://biorender.com/).

Funding:

Parkinson's Foundation-APDA Summer Student Fellowship PF-APDA-SFW-1919, Parkinson Research Consortium (PRC) Summer Studentship, University of Ottawa Faculty of Medicine, Office of Francophones Affairs Scholarship. (JLAP)
Parkinson Research Consortium (PRC) Larry Haffner Fellowship, Parkinson Canada Basic Research Fellowship BRF-2021-0000000048. (KMR)
Parkinson's Research Consortium (PRC) Bonnie and Don Poole Fellowship, Ontario Graduate Scholarship, Queen Elizabeth II Scholarship. (HMG)

Canadian Institutes of Health Research (FRN-153188). (WLS)
Vanier Canada. (MGS)
Parkinson's Society of Southwestern Ontario (PSSO). (BBD)
Canadian Institutes of Health Research (FRN-159443). (SDR)
Parkinson's Foundation Stanley Fahn Junior Faculty Award (PF-JFA-1762), Canadian Institutes of Health Research (PJT-169097), the Parkinson Canada New Investigator Award (2018-00016), Aligning Science Across Parkinson's (ASAP-020625) through the Michael J. Fox Foundation for Parkinson's Research (MJFF). (MWCR)

Author contributions:

Conceptualization: JLAP, KMR, MWCR
Methodology: JLAP, KMR, MS, BBD, EL, BN, NAL, HMG, AB, MGS, BBD, SMC, MWCR
Investigation: JLAP, KMR, MS, BBD, HMG, SMC, MWCR
Supervision: WLS, MGS, SDR, MWCR
Writing – original draft: JLAP, KMR, MWCR
Writing – review & editing: JLAP, KMR, JJT, MGS, WLS, PB, SDR, MWCR
Resources: AJ, PB

Competing interests:

The authors declare that they have no conflict of interest.

Data and materials availability:

All data of this study are in the main text or in the Supplementary Materials. $Cdk14^{+/-}$ and $Cdk14^{-/-}$ mice were obtained from David Park from the University of Calgary and are on an F14 C57BL/6N background. mThy1-SNCA "line 61" (*α-Syn TG*) mice were obtained from Robert Rissman from the University of California, San Diego. Mouse α-Syn PFF preparations were provided by Patrik Brundin, Van Andel Institute, Grand Rapids. Any other materials are commercially available.

773 **Figures**

774 **Figure 1. Loss of Cdk14 ameliorates motor impairment and α-Syn pathology in PFF-injected**
775 **mice.** (A) Mouse α-Syn PFFs were injected unilaterally to the striatum by stereotactic injection in
776 6-month-old mice. (B) Loss of forelimb grip strength at 6 months post α-Syn PFF-treatment in
777 WT mice, but not in *Cdk14*$^{+/-}$- or *Cdk14*$^{-/-}$-mice. Two-way ANOVA, Bonferroni *post hoc,* n: 9-10.
778 (C) α-Syn PFF-injection increased the load of pS129 α-Syn-positive cells (depicted without and
779 with hematoxylin counterstaining, 50 µm scale bars) in the injected hemisphere (ipsilateral, IL).
780 Densities of pS129 α-Syn-positive cells are depicted in heat maps as hues of red at 3 rostrocaudal
781 levels (relative to bregma: +0.98 mm, +0.26 mm, and -1.34 mm) with dark shades of red
782 correlating to high cell densities. Amounts of pS129 α-Syn-positive cells in all brain regions
783 (averaged) and the somatomotor cortex at +0.26 mm relative to bregma of PFF-injected *Cdk14*$^{+/-}$
784 - and *Cdk14*$^{-/-}$- mice were lower relative to their wildtype (WT) counterparts. Two-way ANOVA,
785 Bonferroni *post hoc* comparisons, n: 3-6.

786

787 **Figure 2. Cdk14 modulates PD-like behavior and regulates α-Syn levels in mice**
788 **overexpressing human α-Syn.** (A) Breeding strategy to obtain *α-Syn TG; Cdk14*$^{+/-}$-mice. (B)
789 Elevated turn latencies during pole test experiments were observed in *α-Syn TG*-, but not in *α-Syn*
790 *TG; Cdk14*$^{+/-}$-mice. Two-way ANOVA, Bonferroni *post hoc* comparisons. (C) *α-Syn TG*- and *α-*
791 *Syn TG; Cdk14*$^{+/-}$-mice display similar hyperactive locomotion in beam break experiments when
792 compared to WT mice. Repeated measures two-way ANOVA, Bonferroni *post hoc* comparisons.
793 (D) Nest building quality is similarly reduced in 3-monht-old *α-Syn TG*- and *α-Syn TG; Cdk14*$^{+/-}$-
794 mice. Two-way ANOVA, Bonferroni *post hoc* comparisons, n: 15-19. (E) Immunoblots depicting
795 the levels of pS129 α-Syn, total α-Syn, Cdk14, and GAPDH in the NETN buffer-soluble and -

insoluble protein fraction of mouse hemibrains. Brains of *Cdk14*$^{+/-}$-mice contain less total α-Syn than brains of WT mice. Partial ablation of *Cdk14* in *α-Syn TG* results in elevated levels of pS129 α-Syn in the soluble fraction and decreased total α-Syn levels in the insoluble fraction. Unpaired student's *t* tests, n:5-7.

Figure 3. Genetic reduction of Cdk14 prevents neuron loss in *α-Syn TG* mice and mildens α-Syn pathology in human neurons. Immunofluorescence staining for NeuN in the Ca3 region of the hippocampus (A, 200 µm scale bar) and layer V of the cortex (B, 100 µm scale bar) visualize reduced neuronal densities in *α-Syn TG* mice which is not observed in *α-Syn TG; Cdk14*$^{+/-}$-mice. Two-way ANOVA, Bonferroni *post hoc* comparisons, n=5. (C) Immunoblots illustrating elevated amounts of pS129 α-Syn in hiPSC-derived *SNCA* A53T human neurons (in comparison to isogenic corrected neurons [Corr]) which is reduced by CRISPR/Cas9-mediated knockdown of *CDK14* (targeted against *CDK14* exon 3 (E3) and 8 (E8)). One-way ANOVA, Tukey *post hoc* comparisons, n=3-4.

Figure 4. Pharmacological inhibition of CDK14 reduces α-Syn protein burdens in human and rodent neurons. (A) Application of 500 nM of the CDK14 inhibitor FMF-04-159-2 for 18 hours to HEK293T cells decreases CDK14 and α-Syn levels, as shown by immunoblots. Unpaired student's *t* tests, n=6. (B) Dose-dependent reduction of α-Syn in hESC-derived human neurons is detected by ELISA quantification after 72 hours of CDK14 inhibitor treatment. One-way ANOVA, Bonferroni *post hoc* comparisons, n=3. (C) Human α-Syn PFFs applied to rat cortical neurons increase the amount of α-Syn, as shown by immunoblots, which was reduced by the application of

818 100 nM of the CDK14 inhibitor for 5 days. Repeated measures one-way ANOVA, followed by

819 Holm-Šídák *post hoc* comparisons, n=3.

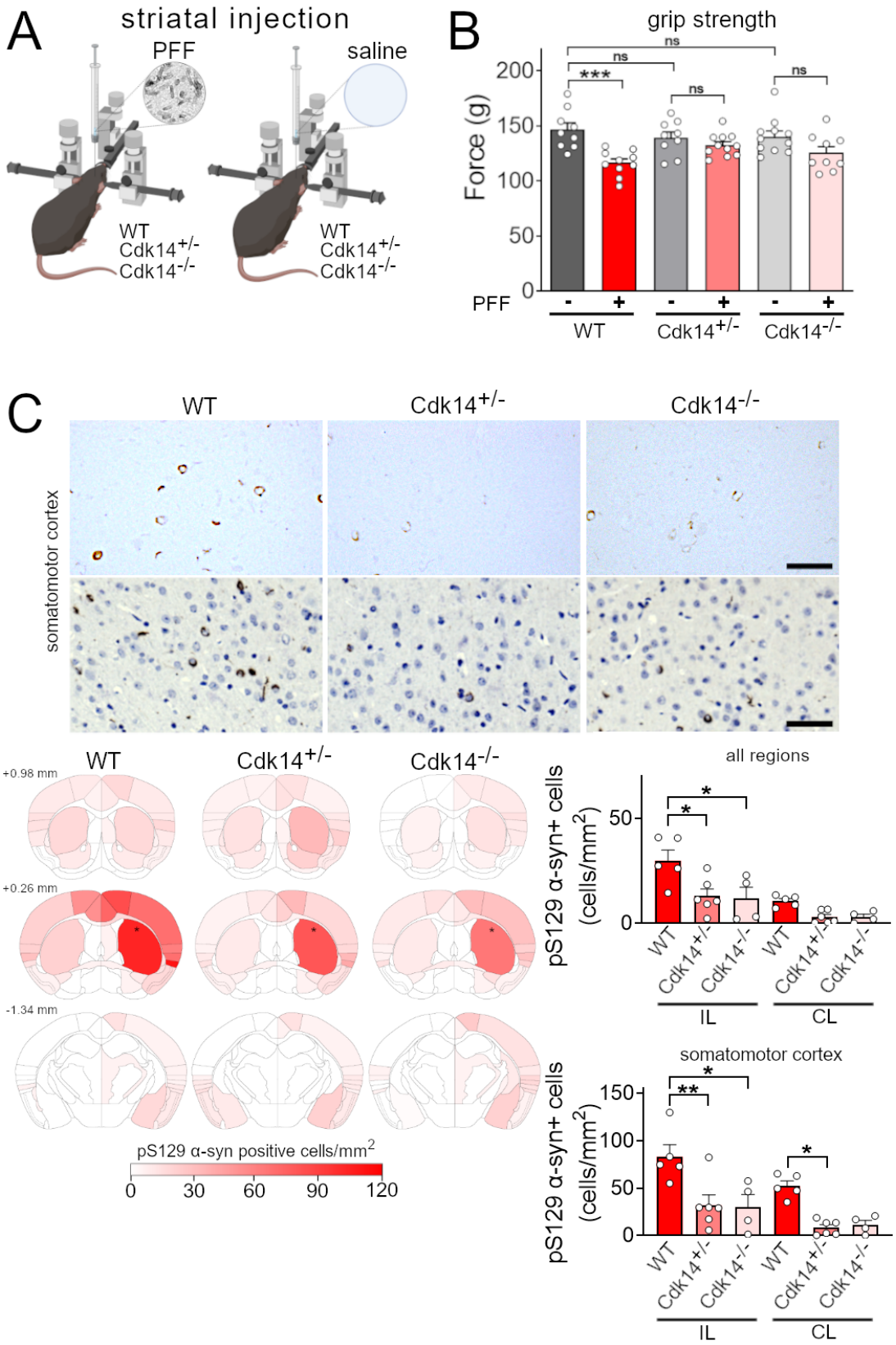

820

821 **Fig. 1**

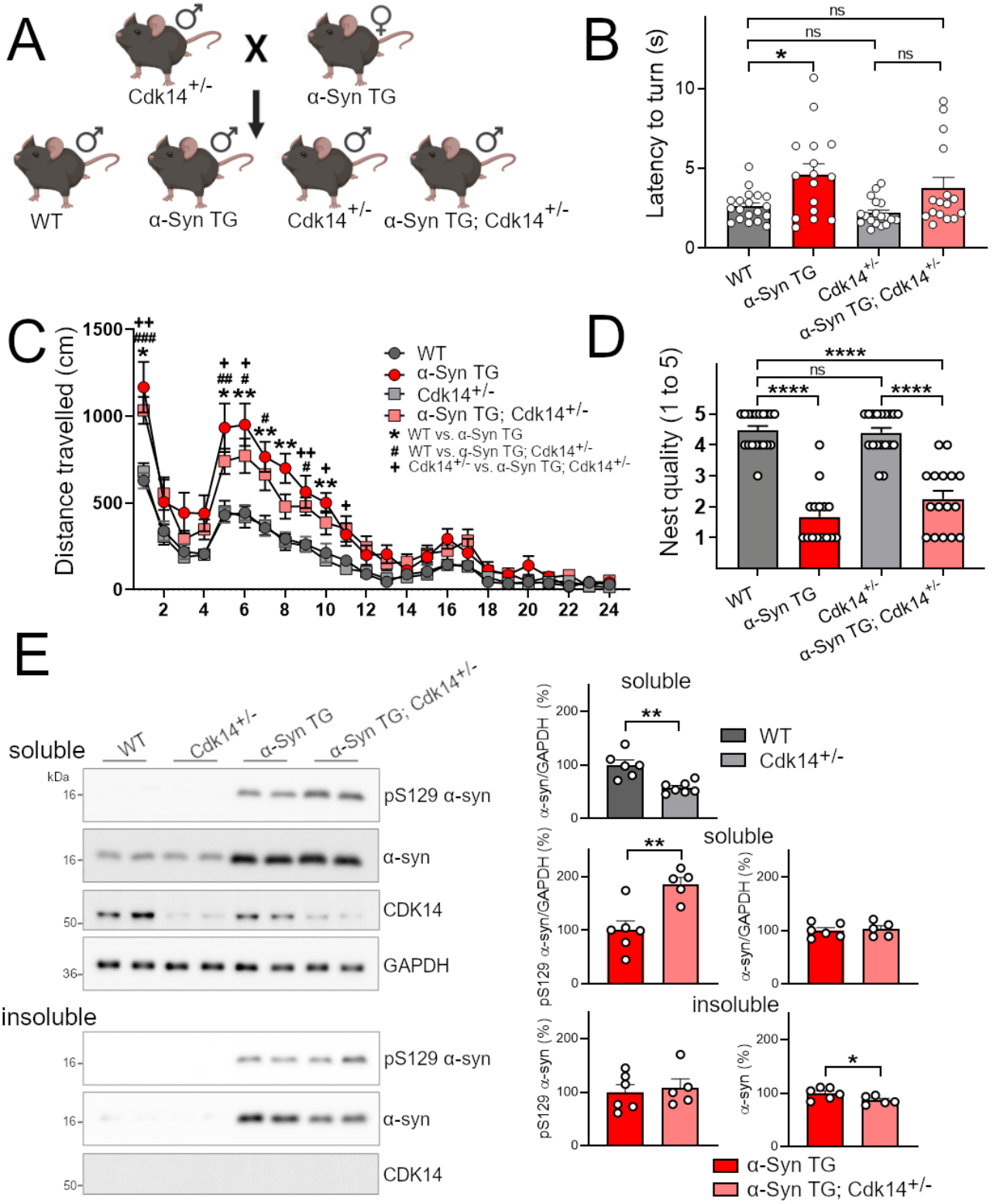

Fig. 2

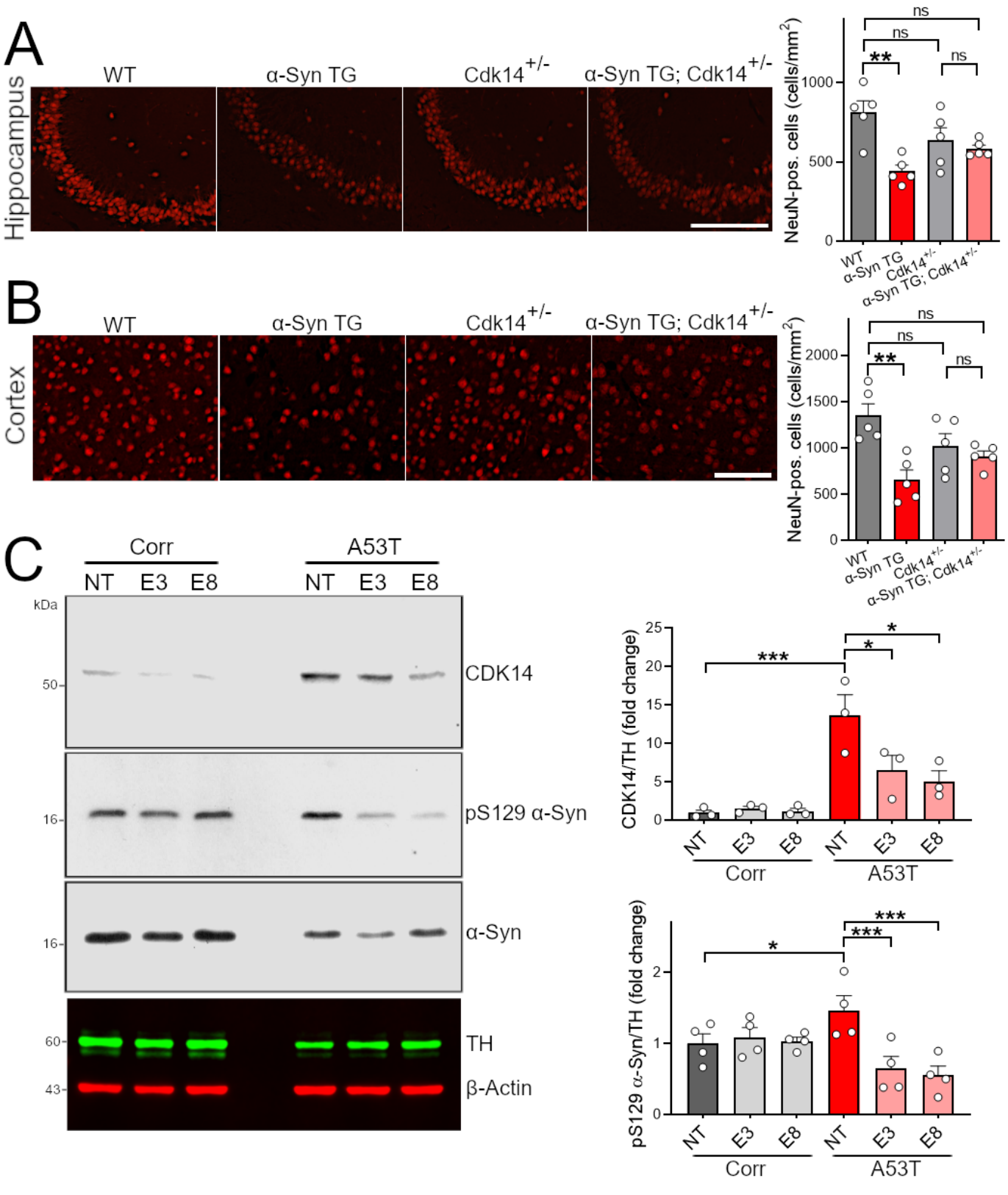

824

825 **Fig. 3**

826

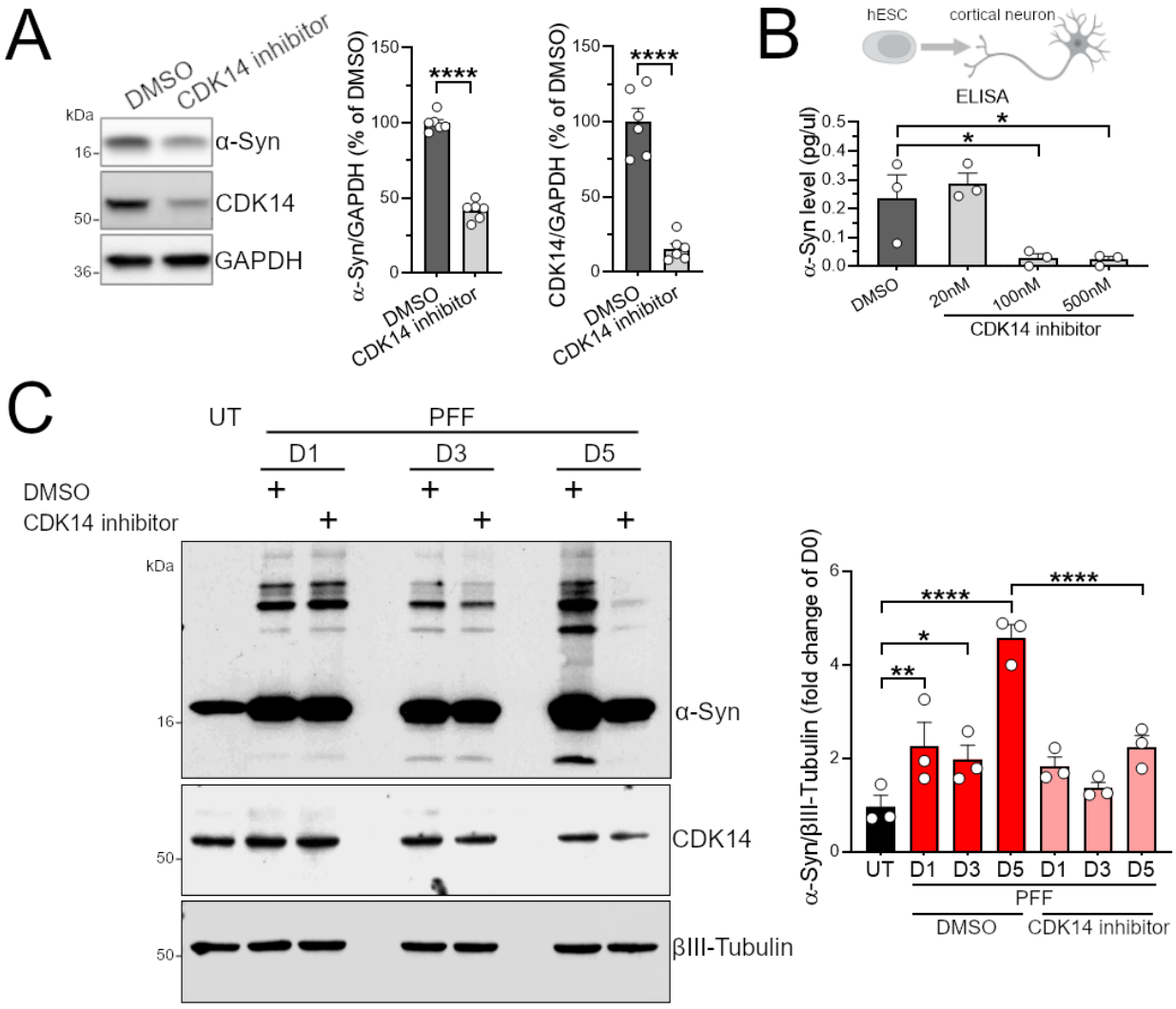

827

828 **Fig. 4**

829

Supplementary Materials

Figure S1. Cdk14 protein levels in mouse organs and mouse α-Syn PFF characterization. (A) Immunoblots depicting Cdk14 protein from different organs of *Cdk14*$^{-/-}$- and WT-mice. (B) Transmission electron micrograph (500 nm scale) illustrating mouse α-Syn PFFs used for intrastriatal injections and corresponding α-Syn PFF length analysis.

Figure S2. Behavioral profile and dopaminergic striatal fiber density of PFF injected *Cdk14*$^{-/-}$-mice. (A) 12-month-old *Cdk14*$^{+/-}$ and *Cdk14*$^{-/-}$- mice do not display altered behavior in the nesting, tail suspension, elevated plus maze, Y maze, open field, hanging wire, pole (two-way ANOVA, Bonferroni *post hoc* comparisons) and rotarod test (repeated measures two-way ANOVA, Bonferroni *post hoc* comparisons, n:9-10). PFF treatment does not result in significant changes of behavior at 6 months post injection. (B) PFF injection does not change striatal tyrosine hydroxylase (TH)-positive fiber density in the ipsilateral side (IL) in comparison to the non-injected, contralateral side (CL) at bregma 0.26 mm (200 µm scale). Two-way ANOVA, Bonferroni *post hoc* comparisons, n: 3-7.

Figure S3. Histopathology in *α-Syn TG; Cdk14*$^{+/-}$-mice and α-Syn protein levels in rat primary neurons. (A) Cortical pS129 α-Syn signal intensities do not differ between *α-Syn TG*- and *α-Syn TG; Cdk14*$^{+/-}$-mice (200 µm scale). Two-way ANOVA, Bonferroni *post hoc* comparisons, n=4-5. (B) *α-Syn TG*- and *α-Syn TG; Cdk14*$^{+/-}$-mice display similar degrees of astrogliosis in the hippocampus, visualized by GFAP staining (200 µm scale). Two-way ANOVA, Bonferroni *post hoc* comparisons, n=5. (C) For protein degradation experiments, HEK293T cells

were treated with 500 nM FMF-04-159-2, 1 μM MG-132 and 200 nM Bafilomycin A1 for 18 hours. Activity of the ubiquitin proteasome system and autophagy is visualized with immunoblots by Ubiquitin and LC3B, respectively. Two-way ANOVA, Bonferroni *post hoc* comparisons, n=3. Application of 500 nM of FMF-04-159-2 for 18 hours to HEK293T cells decreases *SNCA* transcript levels, quantified by qPCR. Unpaired student's *t* tests, n=6. (D) Rat cortical neurons treated with α-Syn monomers do not present with elevated amounts of α-Syn monomers. Repeated measures one-way ANOVA, followed by Holm-Šídák *post hoc* comparisons, n=3.

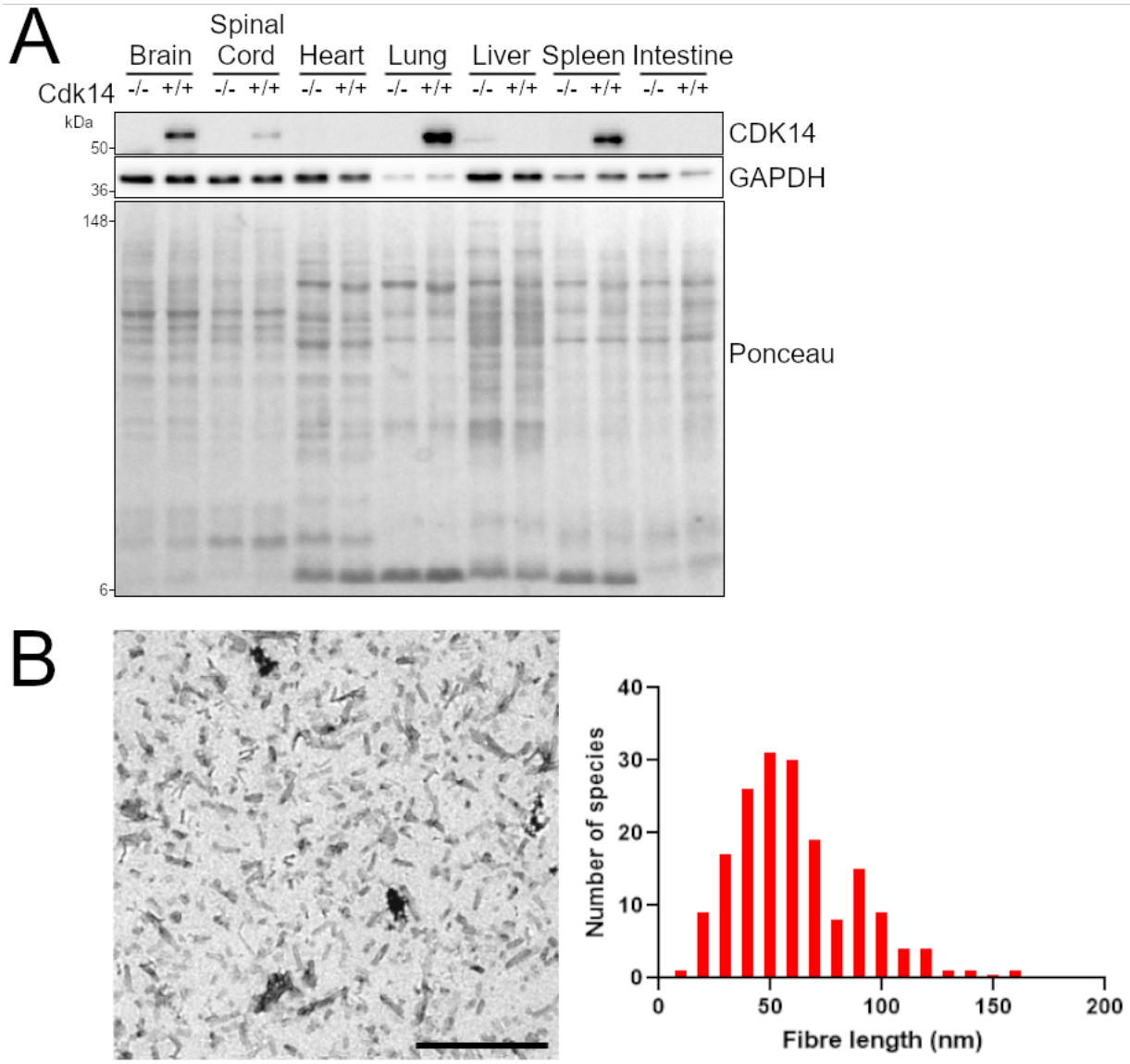

Fig. S1.

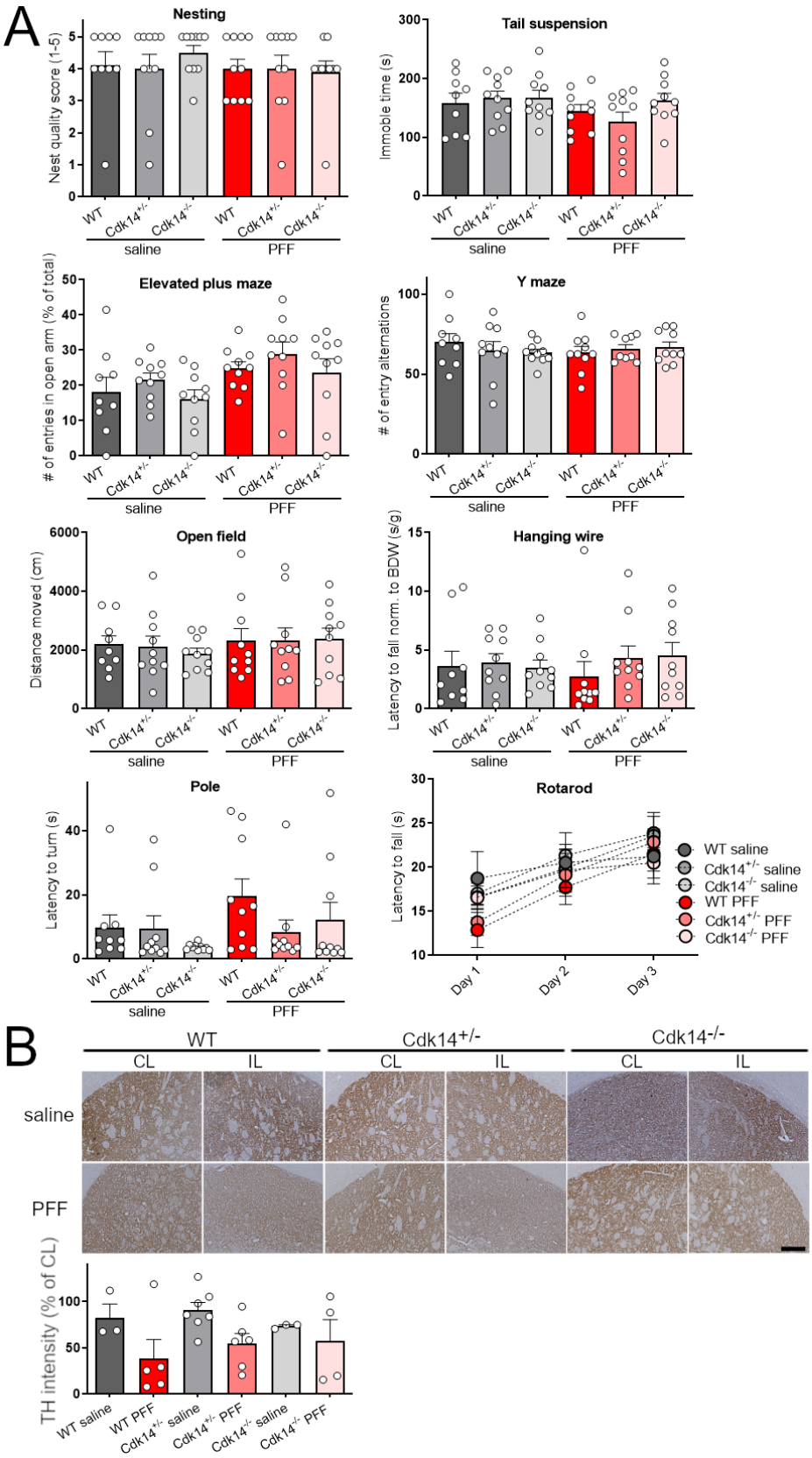

Fig. S2

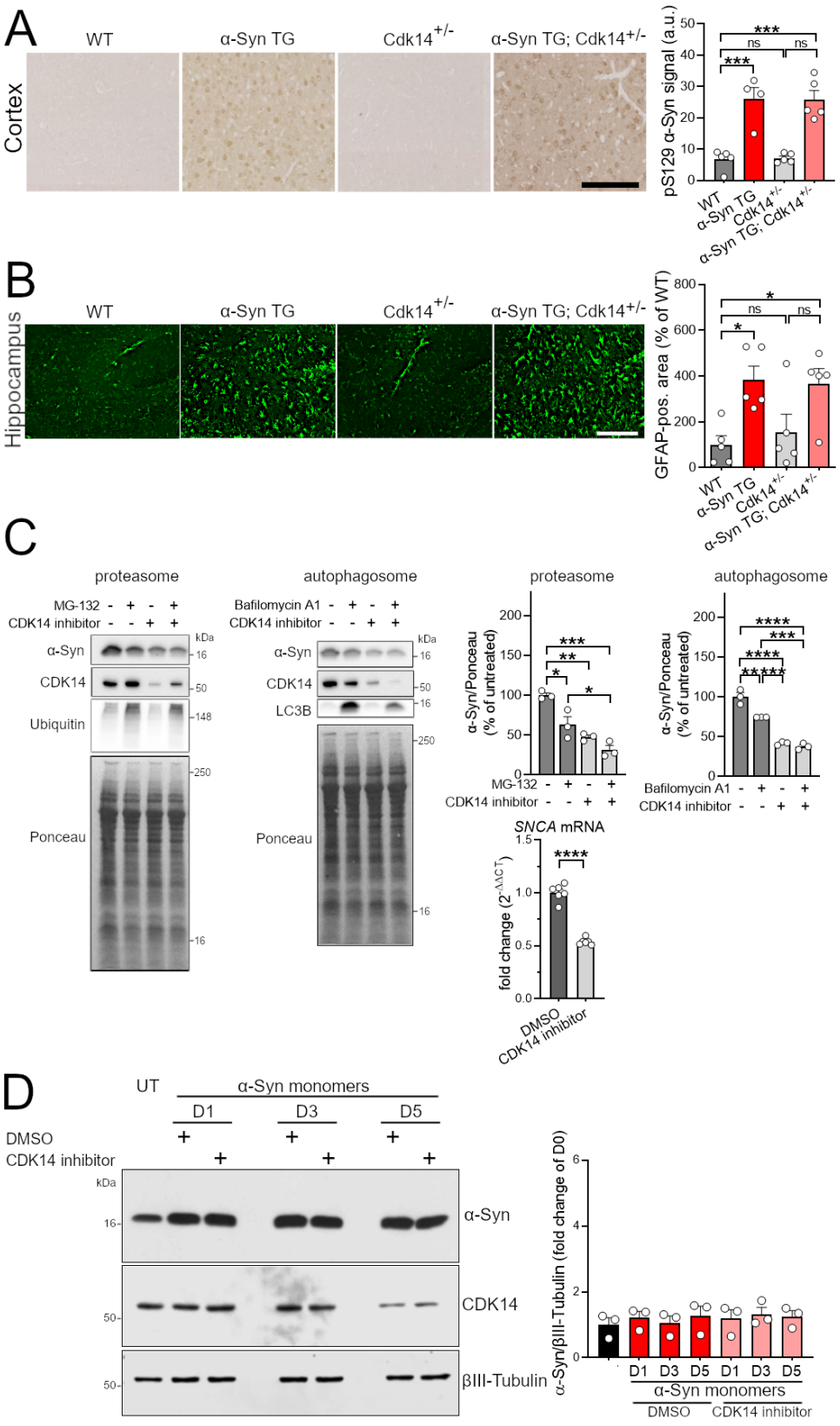

871

872 **Fig. S3**